

## Ultrathin Acoustic Metasurface-Based Schroeder Diffuser

Yifan Zhu,<sup>1</sup> Xudong Fan,<sup>1</sup> Bin Liang,<sup>1,\*</sup> Jianchun Cheng,<sup>1,†</sup> and Yun Jing<sup>2,‡</sup>

<sup>1</sup>Key Laboratory of Modern Acoustics, MOE, Institute of Acoustics, Department of Physics, Collaborative Innovation Center of Advanced Microstructures, Nanjing University, Nanjing 210093, People's Republic of China

<sup>2</sup>Department of Mechanical and Aerospace Engineering, North Carolina State University, Raleigh, North Carolina 27695, USA

(Received 9 December 2016; revised manuscript received 8 March 2017; published 5 June 2017)

“Schroeder diffuser” is a classical design, proposed over 40 years ago, for artificially creating optimal and predictable sound diffuse reflection. It has been widely adopted in architectural acoustics, and it has also shown substantial potential in noise control, ultrasound imaging, microparticle manipulation *et al.* The conventional Schroeder diffuser, however, has a considerable thickness on the order of one wavelength, severely impeding its applications for low-frequency sound. In this paper, a new class of ultrathin and planar Schroeder diffusers are proposed based on the concept of an acoustic metasurface. Both numerical and experimental results demonstrate satisfactory sound diffuse reflection produced from the metasurface-based Schroeder diffuser despite it being approximately 1 order of magnitude thinner than the conventional one. The proposed design not only offers promising building blocks with great potential to profoundly impact architectural acoustics and related fields, but it also constitutes a major step towards real-world applications of acoustic metasurfaces.

DOI: [10.1103/PhysRevX.7.021034](https://doi.org/10.1103/PhysRevX.7.021034)

Subject Areas: Acoustics, Metamaterials

In the 1970s, Schroeder published two seminal papers on sound scattering from maximum-length-sequence and quadratic-residue-sequence diffusers [1,2]. For the first time, a simple recipe was proposed to design sound-phase grating diffusers with defined acoustic performance. These two papers opened a brand-new field of sound diffusers with applications in architectural acoustics [3–5], noise control [6–8], ultrasound imaging [9], and microparticle separation [10] and have inspired other disciplines such as energy-harvesting photodiodes [11]. D’Antonio and Konnert [12] presented one of the most accessible review papers examining the theory behind Schroeder’s diffusers (SDs). Most importantly, they commercialized SDs and promoted them to be widely adopted in architectural acoustics, where the diffusers can be used to spread the reflections into all directions, reducing the strength of the undesired specular reflection and echo, as well as preserving the sound energy in space [3]. In contrast to diffusers, sound absorbers reduce the energy in the room, which can be problematic for unamplified performances in concert halls, opera houses, and auditoria. Sound diffusers are also used to promote

desired reflections in order to enhance spaciousness in auditoria, to improve speech intelligibility, and to reduce the noise on urban streets [3,13,14]. Instead of using a surface with random or geometric reflectors, Schroeder innovatively designed a family of diffusers based on number-theory sequences, with the ultimate goal to produce predictable and optimal scattering (i.e., the sound is scattered evenly in all directions regardless of the angle of incidence). In spite of the great success that SDs have achieved, they are conventionally designed to have a grating structure with a thickness that can be as large as half of the wavelength at the design frequency in order to achieve the desired phase delays. To put this into perspective, the thickness of a SD could reach a remarkable value of 69 cm at 250 Hz, which is in the range of human voices, truck noises, etc. Figure 1(a) shows a simple one-dimensional (1D) SD to illustrate the basic concept of SDs. The bulky size of conventional SDs poses a fundamental limitation on their applicability; i.e., SDs are typically limited to mid- and high frequencies because they are too large to be accommodated at low frequencies, which is a very important part of sound that humans perceive. In addition, SDs usually do not complement the visual appearance of a space because of their large size and irregular surface. Although active methods may offer a solution to this limitation [15], they are much more expensive and complicated and therefore less practical compared to their passive counterpart.

In this paper, we revisit the SD and redesign it using the concept of an acoustic metasurface [16–25]. Despite the considerable efforts dedicated to the research on acoustic metamaterials and acoustic metasurfaces [16–40], they are

\*liangbin@nju.edu.cn

†jccheng@nju.edu.cn

‡yjing2@ncsu.edu

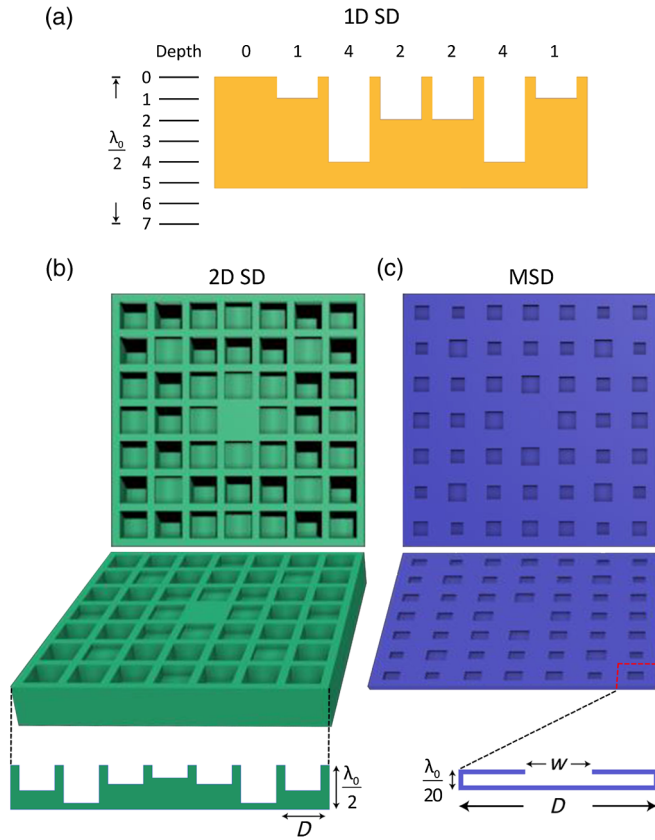


FIG. 1. (a) A one-dimensional Schroeder diffuser (1D SD). The maximum well depth is relatively small in this specific case ( $2\lambda_0/7$ ) because of the small ratio of the largest sequence number 4 to the prime number 7. (b) A 2D SD. (c) The proposed metasurface-based Schroeder diffuser. The top and bottom images in (b) and (c) are the top and 45° angle views of SD and MSD, respectively. The insets in (b) and (c) are the cross sections of unit cells in SD and MSD, with the thicknesses being  $\lambda_0/2$  and  $\lambda_0/20$ , respectively.

still at an embryonic stage from the real-world application perspective. While previous studies on acoustic metamaterials or metasurfaces have revealed interesting physics, there has been a longstanding gap between metamaterials and metasurfaces and how they can be used for real-world applications, therefore severely impeding their further development. One main objective of this study is to fill this gap by examining a new family of metasurfaces under a realistic setup and comparing them with commercially existing products. Metasurfaces are thin structures having subwavelength thickness consisting of unit cells that could give rise to numerous intriguing phenomena such as super sound absorption [16,17], wave-front shaping [18–22], dispersion-free phase engineering [23], and asymmetric acoustic transmission [24,25]. Here, we show the potential of using acoustic metasurfaces to break down the fundamental physical barrier in designing ultrathin SDs. As will be demonstrated in this paper, the metasurface-based SD (MSD) has a comparable performance to the conventional

SD that has already been commercialized and widely used in practice. More importantly, the MSD is roughly 1 order of magnitude thinner with a planar configuration and is therefore more suitable for low-frequency applications in architectural acoustics or other related fields. This paper will present the theoretical design, numerical simulation, and experimental demonstration of the ultrathin MSDs with a thickness that is  $1/20$  of the center or design frequency wavelength  $\lambda_0$ . The unit cell of the proposed MSD is a locally resonant element having a relatively simple geometry, and its acoustical response can be engineered flexibly and precisely by adjusting a single geometrical parameter, which enables convenient analytical prediction of its acoustical phase response. The metasurface is designed in such a way that the thickness is minimized, while the performance is not significantly affected by the thermal and viscous losses [41,42]. This result is in contrast to the widely studied space-coiling structure-based metasurfaces that may suffer from large losses at a comparable thickness [19–21,23]. Our initial design is further improved by the broadened frequency band introduced by a hybrid structure containing units operating at multiple optimal frequencies. The experimental and simulation results were in good agreement, and both showed that the MSD yielded a performance on par with the conventional SD, despite it being approximately 1 order of magnitude thinner. This study aims to channel the direction of acoustic metamaterials or metasurfaces so that they can be better poised for tackling real-world problems, thereby greatly benefiting the metamaterial-metasurface and acoustic communities.

First, we briefly review the conventional design of SDs and elucidate the fundamental limitation of this design. In order to generate diffuse reflection for different incident acoustic waves, the phase shift at the surface of a SD must yield a specific profile such as a special number sequence [43]. Conventionally, the desired phase delay in a SD is achieved by controlling the sound path in a grating structure, resulting in the fact that the maximum depth of individual units of grating, also referred to as the “well,” can reach half of the wavelength to ensure that the phase changes within a  $2\pi$  range. Figure 1(a) schematically shows a 1D SD formed by a series of wells, which is used for generating diffuse reflections in a two-dimensional (2D) plane; it is called a single plane diffuser [43]. To generate diffuse reflections in three-dimensional (3D) space, one needs to use the 2D model shown in Fig. 1(b). In the 1D case, the depths of the wells are dictated by a mathematical number sequence, such as a quadratic residue sequence (QRS) shown in Fig. 1(a) for which the sequence number for the  $n$ th well,  $S_n$ , is given by [43]

$$S_n = n^2 \text{ modulo } N, \tag{1}$$

where modulo indicates the least non-negative remainder and  $N$  is the number of wells per period. One example of quadratic residue diffusers with  $N = 7$  shown in Fig. 1(a)

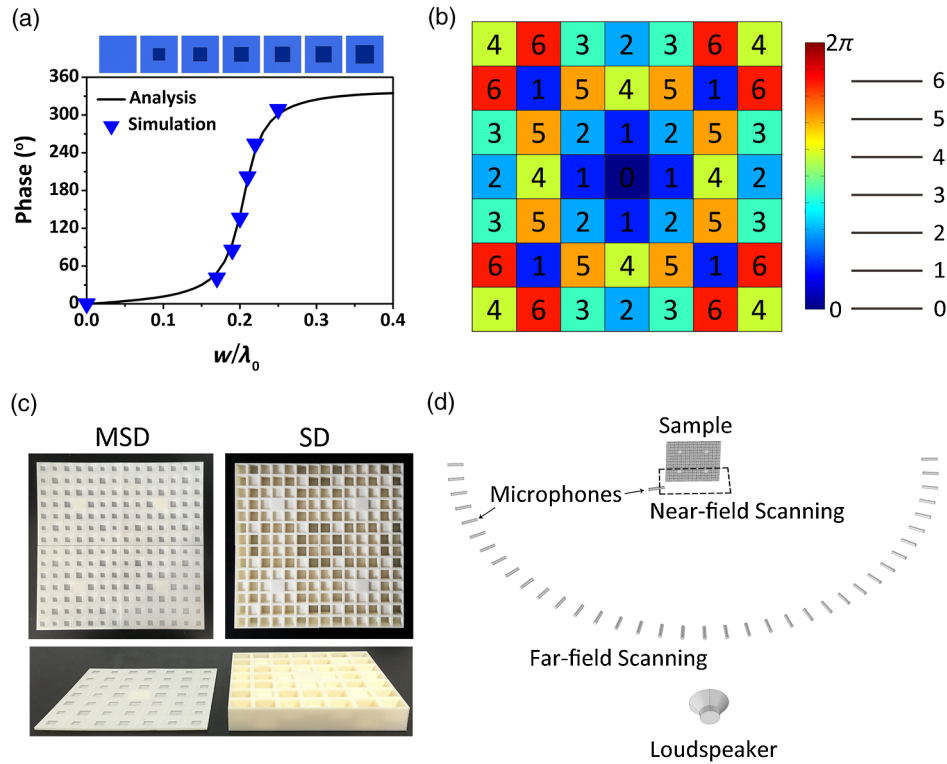


FIG. 2. Design of the metasurface-based Schroeder diffuser. (a) The analytical and simulated relationship between the phase shift and the geometrical parameter  $w$  of the MSD at the center frequency of  $f_0 = 6860$  Hz. The triangles represent the discrete points for generating the phase of  $0-2\pi \times 6/7$  with a step of  $2\pi \times 1/7$ , corresponding to numbers 0–6 in (b). (b) The design of a 2D MSD based on a 2D quadratic residue sequence. One period consists of  $7 \times 7$  unit cells. (c) The photographs of the 3D printed samples of MSD and SD with  $2 \times 2$  periods of QRS, viz.,  $14 \times 14$  unit cells. (d) The schematic diagram of the experimental setup.

has  $S_n = \{0, 1, 4, 2, 2, 4, 1\}$ . The physics of QRS for generating diffuse reflection is detailed in Ref. [12]. QRS has the important property that the Fourier transform of the exponentiated sequence values has constant magnitude. Consequently, all grating lobes will have the same energy. The depth  $h_n$  of the  $n$ th well is then determined from the sequence  $S_n$  using the following equation:

$$h_n = \frac{S_n \lambda_0}{2N}. \quad (2)$$

Consequently, the well depth varies from 0 to approximately  $\lambda_0/2$ . The phase delay that a SD needs to yield was previously considered unattainable by a simple structure with a deep-subwavelength size. Some attempts have been made to reduce the thickness of the SD by using folded L-shaped wells [44–47] and perforated panels [48,49], cutting the thickness by approximately half. Another commercialized design uses T-shaped wells and their associated resonance to improve the low-frequency performance of diffusers [47]. These designs, however, fail to significantly reduce the thickness of the diffuser. Here, we revisit this problem from the perspective of acoustic metasurfaces and demonstrate that it is possible to realize such a phase profile by using properly designed metasurface units at a deep-subwavelength scale in the thickness direction. The

schematic diagram of the proposed MSD is illustrated in Fig. 1(c). The ultrathin MSD is designed to produce the desired scattering fields mimicking those of SDs, via metastructure units shown in the inset of Fig. 1(c). The width and thickness of the unit are  $D = \lambda_0/2$  and  $\lambda_0/20$ , respectively. In this study, the neck width of the cavity  $w$  is the only tunable parameter for controlling the phase shift of the metastructure unit. Although the unit cell is Helmholtz resonator (HR)-like, its cavity width and neck width are much larger than those of the classical HRs with respect to  $\lambda_0$ . Consequently, the well-established analytical theory for classical HRs (e.g., the lumped model) is not valid anymore and must be revisited (please see Ref. [50]).

Figure 2(a) shows the simulated and analytically predicted phase response of the metastructure unit cells for normally incident waves, which provides us with the design for a center frequency at  $f_0 = 6860$  Hz. Note that the phase response depends on the incidence angle, and this is discussed in Ref. [50]. Finite-element-analysis software COMSOL 5.0 is used for numerical simulations. The relatively high frequency chosen in this study is merely for the convenience and precision of experimental characterization. (The low-frequency performance is difficult to characterize experimentally due to the fact that the requirement on the far field is challenging to fulfill.) Our design,

however, is readily scalable and could easily be applied to any audible frequency of interest. The simulation results for the design at  $f_0 = 343$  Hz are shown in Ref. [50] to verify the scalability of our scheme. By adjusting a single parameter  $w$ , an almost full  $2\pi$  control of reflected phase can be achieved, as shown in Fig. 2(a). The triangles in Fig. 2(a) mark the parameters of the prototype diffuser based on the simulated result. The seven discrete phases [which correspond to numbers 0–6 in Fig. 2(b)] represent phases of  $0-2\pi \times 6/7$  with a step of  $2\pi \times 1/7$ . We then design a QRS for a 2D sample with  $N = 7$ , and the sequence number  $S_{n,m}$  can be expressed as [43]

$$S_{n,m} = (n^2 + m^2) \text{Modulo } N, \quad (3)$$

where  $n$  and  $m$  represent the row and column numbers of the unit cells. The largest well depth for a corresponding SD is consequently  $3\lambda_0/7$ . Taking into account the backing-plate thickness, the total thickness of the SD is close to  $\lambda_0/2$ . For generating the same scattering effect as conventional SDs, the phase response of the MSD unit cells can be expressed as

$$\phi_{n,m} = \frac{2\pi[(n^2 + m^2) \text{modulo } N]}{N}. \quad (4)$$

The corresponding 2D QRS is shown in Fig. 2(b). This QRS is obtained with indices  $n$  and  $m$  starting from 4 (in order to place the zero depth well at the center of the diffuser) in Eq. (3). The photograph of a 3D-printed MSD and a SD sample with  $2 \times 2$  periods (one period is defined as  $7 \times 7$  unit cells corresponding to one full QRS) is shown in Fig. 2(c). The material is acrylonitrile-butadiene-styrene (ABS) plastics with density  $\rho = 1180$  kg/m<sup>3</sup> and sound speed  $c = 2700$  m/s, which are much larger than those of air, i.e.,  $\rho_0 = 1.21$  kg/m<sup>3</sup> and  $c_0 = 343$  m/s. Figure 2(d) shows the schematic diagram of the experimental setup, from which the far-field directivity and near-field acoustic pressure distributions can be measured. The acoustic field scanning is accomplished by a measuring system consisting of Brüel&Kjær pulse type 3160 and two 0.25-inch-diameter Brüel&Kjær type-4961 microphones.

Figures 3 and 4 show the numerical and experimental results of the MSD and SD samples for normal incidence and  $45^\circ$  incidence angles, respectively. Figure 3(a) shows the simulated 3D far-field scattering patterns of the MSD, SD, and a reference flat plate with the same overall size (marked as “Plate”). Figure 3(b) shows the measured (upper) and simulated (lower) near-field scattered-acoustic-pressure field distributions of the MSD, SD, and plate in the  $x$ - $z$  plane. The acoustic energy is scattered into different directions after impinging upon the sample. Numerous side lobes with similar magnitudes can be observed, and diffuse reflection can be effectively realized by the sample. This is more pronounced in Fig. 3(c), which shows the simulated and the measured far-field scattering

directivity of the sample (polar response). The reflected fields of the flat plate in Figs. 3(b) and 3(c) show that the reflected wave is scattered primarily into a single direction, as expected because of specular reflection. The comparison between these results shows the effectiveness of our MSD sample at the operating frequency compared with the SD. Similarly, the corresponding results at a  $45^\circ$  incidence angle are shown in Fig. 4 (the arrows mark the incidence directions), and a satisfactory diffuse reflection effect can also be observed for the MSD. In this case, we also measure and simulate the results in the  $y$ - $z$  plane. Results are shown in Fig. 4(c).

In order to quantitatively evaluate the performance of the MSD, we use a parameter called the normalized diffusion coefficient [43,51]:

$$d_n(\theta) = \frac{d(\theta) - d^r(\theta)}{1 - d^r(\theta)}, \quad (5)$$

where  $d(\theta)$  and  $d^r(\theta)$  are the diffusion coefficients of the sample and the reference flat surface, which can be computed using the equation below [43,51]:

$$d(\theta) = \frac{(\sum_{i=1}^M 10^{L_i(\theta)/10})^2 - \sum_{i=1}^M (10^{L_i(\theta)/10})^2}{(M-1) \sum_{i=1}^M (10^{L_i(\theta)/10})^2}, \quad (6)$$

where  $L_i(\theta)$  are a set of sound pressure levels (SPLs) in the polar response,  $M$  is the number of receivers, and  $\theta$  is the angle of incidence. The diffusion coefficient  $d(\theta)$  is a single number that assesses the uniformity of the polar response. If the same energy is scattered in all directions, the diffusion coefficient is 1 (this is termed complete diffusion). If all the energy is scattered in one direction, the diffusion coefficient is zero [51].

Figures 3(d) and 4(e) show the simulated and measured  $d_n(0^\circ)$  and  $d_n(45^\circ)$  versus frequency for the MSD and conventional SD at normal incidence and  $45^\circ$  incidence angles, respectively. The discrepancy is mainly due to the sample fabrication imperfection, edge scattering, background noise, and inherent microphone errors. The fabrication imperfection is expected to be less of a problem at low frequencies, which are what the proposed diffusers truly target. At lower frequencies, the diffuser structures are larger and thus require less fabrication precision. Also, the simulation assumes a perfect condition (plane wave, no reflection from surrounding objects, perfectly rigid surface, etc.) that cannot be completely satisfied in experiments. The results demonstrate that the MSD has normalized diffusion coefficients comparable with the conventional SD in the vicinity of the center frequency. While the present study uses a period number  $2 \times 2$ , we have performed a series of simulations to investigate the influence of the period number on  $d_n(\theta)$  for the SD and MSD, and the results can be found in Ref. [50].

Since the MSD is featured with a subwavelength characteristic, the thermal-viscous effect [41,42] could have a nontrivial effect on the performance of the diffuser.

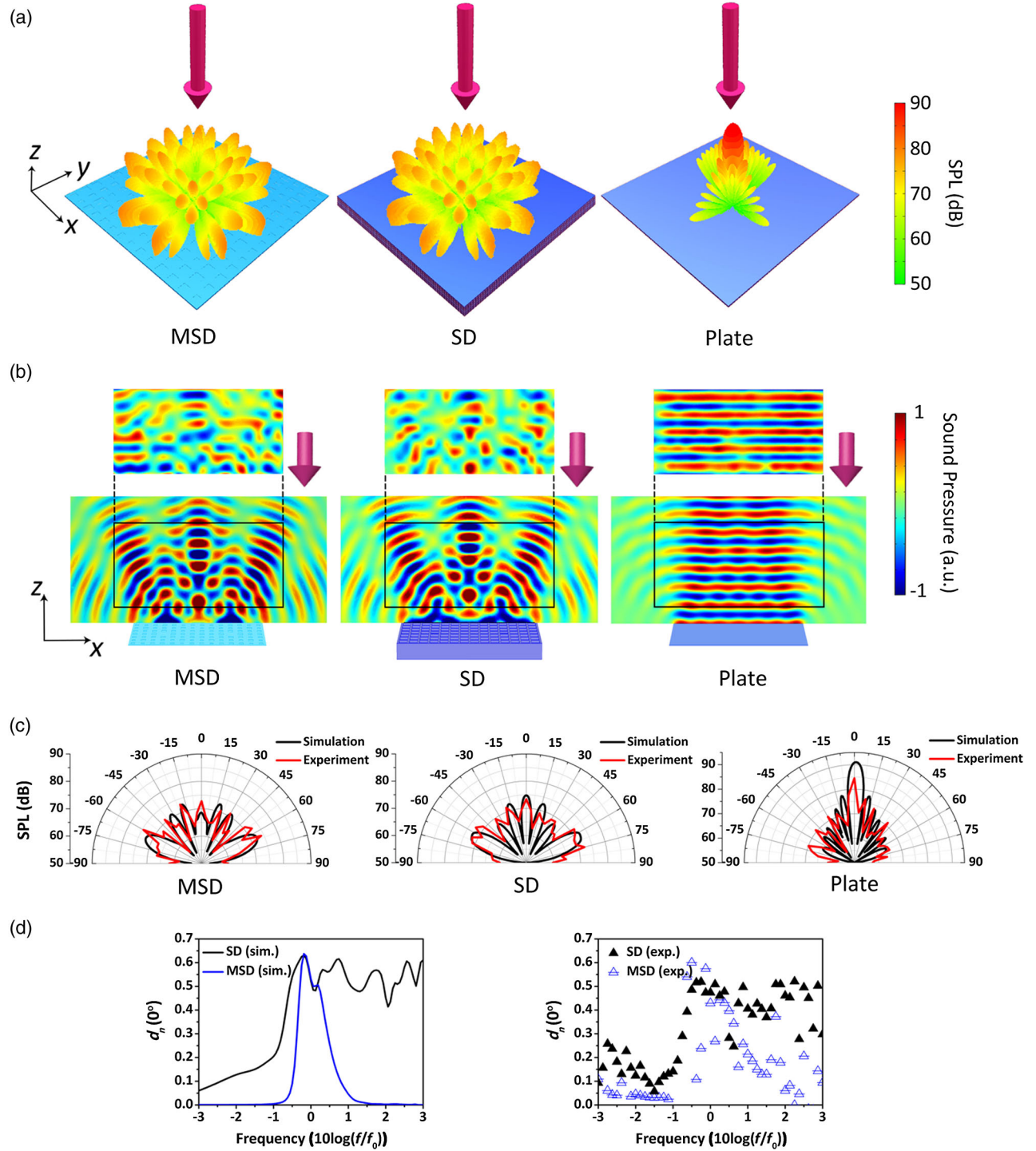


FIG. 3. Simulation and experimental results of the MSD for normal incidence. (a) The simulated three-dimensional far-field scattering patterns of the MSD, SD, and flat plane with normal incidence. (b) The measured (upper) and simulated (lower) scattered acoustic field distributions of the MSD, SD, and flat plate in the  $x$ - $z$  plane. (c) The simulated and measured scattering field directivity of the MSD, SD, and plate. (d) Simulated and measured normalized diffusion coefficient  $d_n(0^\circ)$  versus frequency for the MSD and SD, respectively.

We have numerically investigated the effect of thermal and viscous losses in Ref. [50] and found that these losses do not significantly change the scattering field. A comparison between the Helmholtz-like resonator unit cells and the widely used space-coiling unit cells is also presented

therein, which reveals that the latter yield larger losses. Finally, as mentioned earlier, the unit cells are based on Helmholtz-like resonators because of their relatively large neck widths (up to  $\lambda_0/4$ ), while conventional HRs have neck widths on the deep-subwavelength scale. This is why

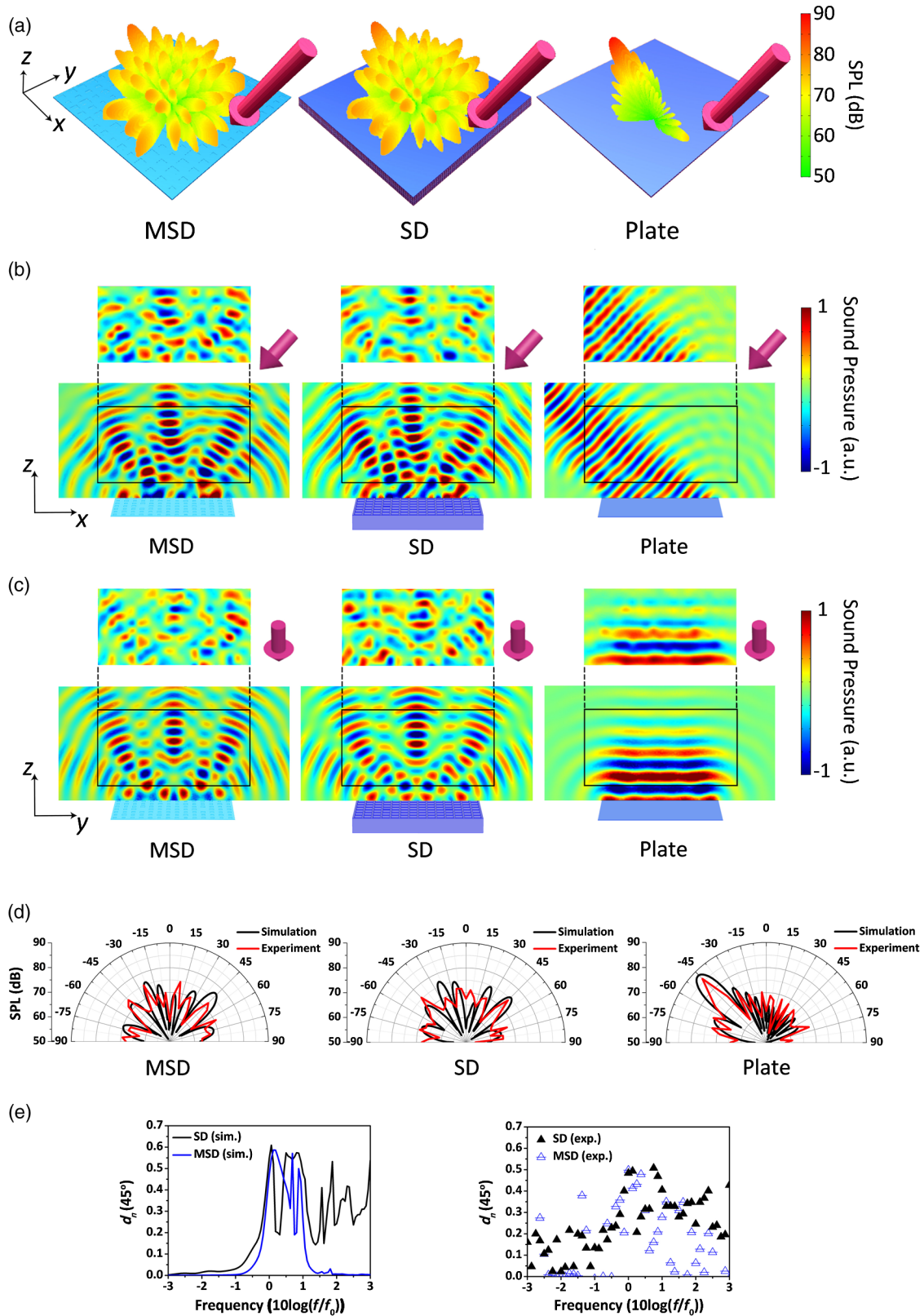


FIG. 4. Simulation and experimental results for oblique incidence. The arrows mark the incidence. (a) The simulated three-dimensional far-field scattering patterns of the MSD, SD, and flat plane with 45° incidence. (b) The measured (upper) and simulated (lower) scattered acoustic field distributions of the MSD, SD, and flat plate in the  $x-z$  plane. (c) The corresponding scattered acoustic field distributions in the  $y-z$  plane. (d) The simulated and measured scattering field directivity of the MSD, SD, and plate. (e) Simulated and measured normalized diffusion coefficient  $d_n(0^\circ)$  versus frequency for the MSD and SD, respectively.

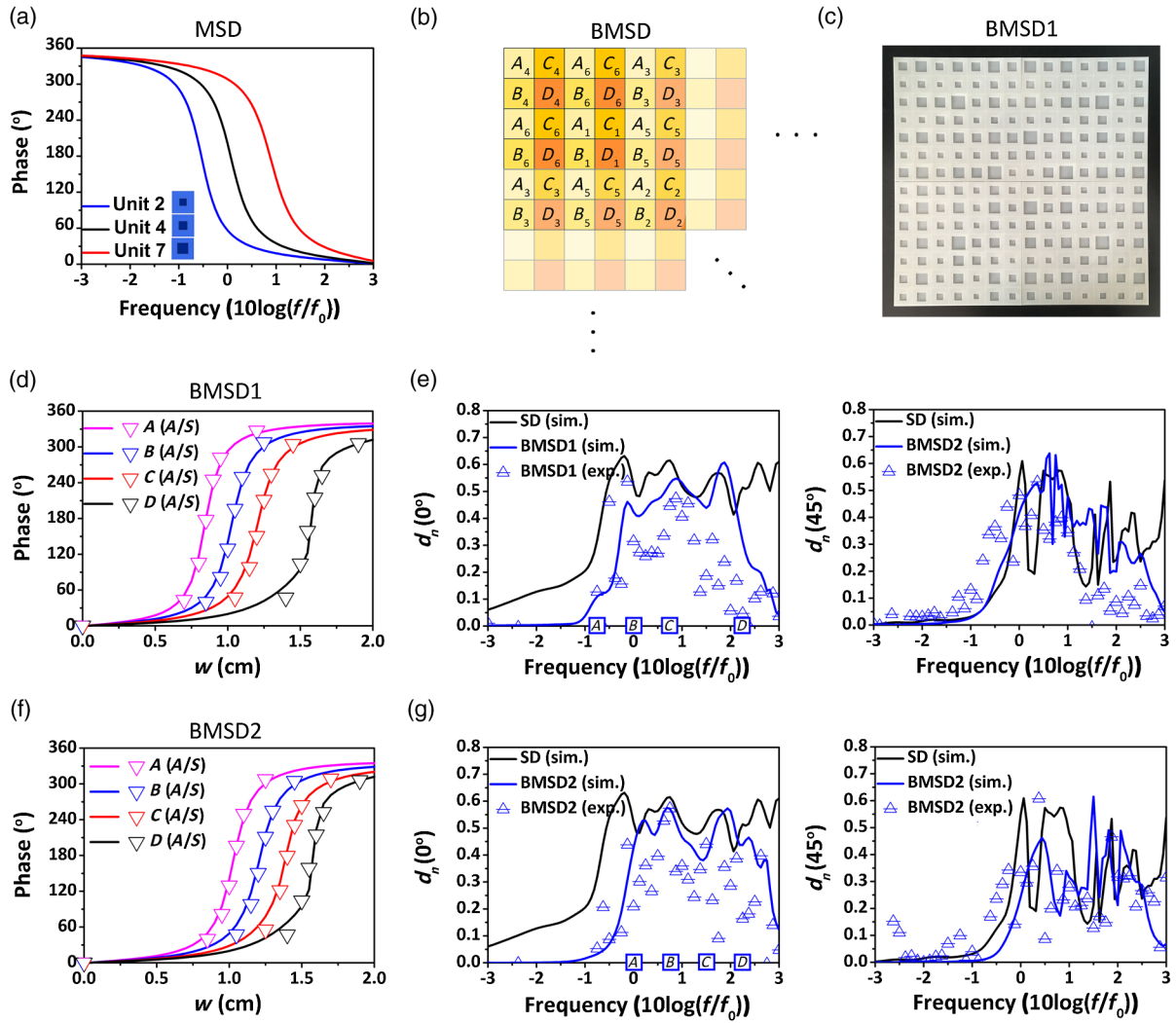


FIG. 5. (a) Phase profile of three selected unit cells of the MSD. Design of broadband metasurface-based Schroeder diffuser. (b) The QRS for a BMSD.  $A_n$ ,  $B_n$ ,  $C_n$ , and  $D_n$  represent four targeted frequencies. (c) Photograph of a 3D printed BMSD1 sample. (d) The analytical and simulated (A/S) relationship between the reflected wave phase and the parameter  $w$  for four frequency components for BMSD1. (e) Simulated and measured  $d_{0,n}$  (left) and  $d_{45,n}$  (right) in the  $x$ - $z$  plane versus frequency for BMSD1 and SD, respectively. The corresponding results for BMSD2 are shown in (f) and (g). In (e) and (g), the center frequency is  $f_0 = 6860$  Hz. The four design frequencies of BMSD1 and BMSD2 are marked by squares A, B, C, and D in (e) and (g), respectively.

the thickness of the metasurface can be minimized without having to suffer from the adverse effects of the boundary-layer-induced loss. Indeed, to the best of our knowledge, the thickness of  $\lambda_0/20$  is the smallest that has ever been reported for acoustic metasurfaces manipulating transmitted or reflected waves with experimental verification (excluding the acoustic metasurfaces for absorption purposes).

We have demonstrated that MSDs can be designed to achieve efficient acoustic diffuse reflection in the vicinity of the center frequency. This initial design suffers from the relatively narrow bandwidth due to the resonance nature of the unit cell. This can also be understood from the rapidly changing phase profile of the unit cells around the design frequency, as shown in Fig. 5(a), which is pivotal for achieving the desired phase change for the reflected wave at

a deep subwavelength depth. To further elucidate this, the Helmholtz-like resonators (locally resonant unit cells) are designed to have a resonance frequency (each unit cell has a different resonance frequency though) close to the design frequency of the diffuser, with unit cells 4 and 5 being closest to the resonance state at the design frequency. Because the reflected wave undergoes a dramatic phase change when the resonators are operating close to the locally resonance state, it is possible to design deep subwavelength unit cells that can cover a wide phase change of  $2\pi$ . We further enhance the MSD by broadening the operating frequency range, which is crucial for certain practical applications. A broadband MSD (BMSD) has a hybrid structure comprising components designed for generating the desired phase delay at multiple frequencies. The multifrequency QRS is shown in

Fig. 5(b), in which  $A_n, B_n, C_n,$  and  $D_n$  represent four different target frequencies and the subscript  $n$  represents the number in QRS.

In this manner, the staggered units for four operating frequencies lead to the BMSD design that targets different frequencies and yields a  $14 \times 14$  array. Figure 5(c) shows the photograph of a BMSD sample. We designed two samples [denoted as BMSD1 and BMSD2 in Figs. 5(d) and 5(f)] with different target frequencies. Figure 5(d) shows the unit parameters of BMSD1 for realizing seven discrete phases in the range  $0 - 2\pi \times 6/7$ . Figure 5(e) shows the numerical

and experimental results of  $d_n(0^\circ)$  and  $d_n(45^\circ)$  in the  $x$ - $z$  plane versus frequency for the SD and BMSD, respectively. The four design frequencies are marked at the coordinate axis of Fig. 5(e), that is, 5772 Hz, 6860 Hz, 8153 Hz, and 11517 Hz for BMSD1 ( $10 \log(f/f_0) = -0.75, 0, 0.75, 2.25$ ). These frequencies are chosen to cover a certain frequency band. Other frequencies within this bandwidth that are sufficiently separated should, in principle, also work. The design frequency for the reference SD is 6860 Hz. The corresponding results for BMSD2 are shown in Figs. 5(f) and 5(g), with the design frequencies being 6860 Hz,

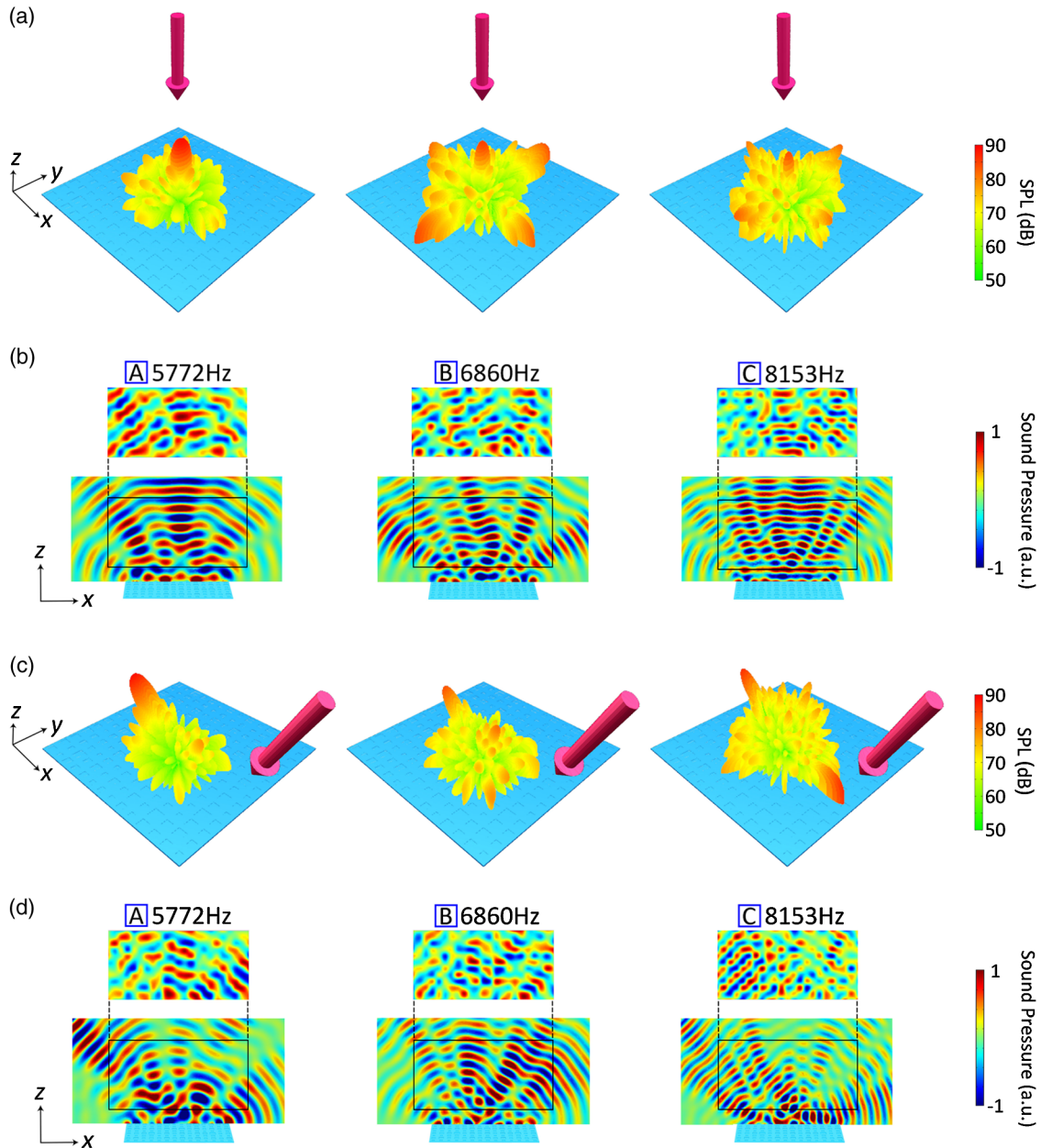


FIG. 6. Simulation and experimental results of the BMSD. (a) The simulated three-dimensional far-field scattering patterns of BMSD1 in the  $x$ - $z$  plane at 5772 Hz, 6860 Hz, and 8153 Hz, respectively, with normal incidence. (b) The measured (upper) and simulated (lower) scattered acoustic pressure fields of BMSD1 in the  $x$ - $z$  plane. The corresponding results for  $45^\circ$  incidence angles are shown in (c) and (d).

8153 Hz, 9690 Hz, and 11517 Hz [ $10 \log(f/f_0) = 0, 0.75, 1.5, 2.25$ ]. The diffuser thickness 0.25 cm is unchanged, and again, the results presented here can be scaled to lower frequencies without extra effort.

In order to characterize the broadband performance of the BMSD samples, we calculate the average normalized diffusion coefficient as

$$d_n(\theta, f_1, f_M) = \frac{\sum_{i=1}^M d_n(\theta, f_i)}{M}, \quad (7)$$

where  $d_n(\theta, f_i)$  is the normalized diffusion coefficient at different discrete frequencies of  $f_i$ ;  $f_1$  and  $f_M$  are the lower and upper bound frequencies of the frequency range of interest, respectively; and  $M$  is the number of simulated discrete frequencies (e.g., we have simulated 13 evenly spaced frequencies within 6292 Hz–7479 Hz for MSD). Comparing SD and MSD, the simulated (measured)  $d_n(0^\circ, 6292, 7479)$  are 0.56 (0.48) and 0.50 (0.36), respectively. The simulated (measured)  $d_n(45^\circ, 6292, 7479)$  are 0.35 (0.34) and 0.37 (0.39), respectively. These results suggest that the MSD have comparable performance as the SD in a relatively small frequency range. In a larger frequency range (here, 6860 Hz–11517 Hz covers the targeted frequencies of BMSD1 and BMSD2 with 37 evenly spaced frequencies), the coefficients for SD, MSD, BMSD1, and BMSD2 are 0.53 (0.42), 0.15 (0.23), 0.51 (0.28), and 0.49 (0.33), respectively, and  $d_n(45^\circ, 6860, 11517)$  are 0.38 (0.34), 0.22 (0.23), 0.34 (0.25), and 0.36 (0.28), respectively. While the SD still performs fairly well due to the fact that at different frequencies the phase response at the surface of the SD is also a “random” distribution, the performance of MSD deteriorates dramatically. On the other hand, the performance of the BMSD is comparable to the SD, although it is roughly 1 order of magnitude thinner. Figure 6 maps the simulated 3D far-field scattering patterns and the measured and simulated near-field scattered acoustic pressure fields for BMSD1 in the  $x$ - $z$  plane for normal incidence and  $45^\circ$  incidence angles at 5772 Hz, 6860 Hz, and 8153 Hz, respectively. The experiment results and simulation results are in reasonable agreement. The scattered acoustic fields show that the BMSD yields diffuse reflection at different frequencies. The results suggest that the bandwidth can be broadened by using the BMSD structure, and the performance is on par with the widely commercialized SD.

In conclusion, we have designed an ultrathin Schroeder diffuser based on the concept of acoustic metasurfaces. A 2D array of locally resonant elements, each generating a specific phase change in its reflected waves, is arranged according to Schroeder’s theory, and an ultrathin version of the SD with a thickness of  $\lambda_0/20$  (roughly 1 order of magnitude smaller than that of conventional SDs) has been successfully demonstrated. Such a deep subwavelength depth is made possible by utilizing Helmholtz-like resonators with relatively wide necks which yield significantly less loss than the conventional Helmholtz resonators. The

proposed diffuser, in theory, can be designed to be even thinner, with the caveat in mind that thermal and viscous losses will become more dominant and introduce excessive absorptions, which could be unwanted in architectural acoustic applications. On the other hand, these additional absorptions may enable hybrid surfaces with simultaneous diffusion and absorption, which can find utility in noise control or in places such as studios where both low reverberation and sound uniformity are desired. We have also proposed a hybrid structure containing units operating at different frequencies in order to broaden the bandwidth of the MSD. The numerical and experimental results both show sound diffuse reflection comparable with the conventional SD. While our study has examined one possible scheme to broaden the bandwidth of the MSD, other feasible schemes will be exploited in the near future under the framework established by this work, including iterative optimization and fractals [43]. Our work takes a first step in applying acoustic metasurfaces to solving practical acoustic problems. The conventional sound diffuser that has been widely adopted in industry is markedly improved by new designs. Our findings may provide a roadmap to manipulate sound scattering and have far-reaching implications in architectural acoustics, noise control, and beyond.

## ACKNOWLEDGEMENTS

We thank Dr. Likun Zhang for helpful discussions. This work was supported by the National Natural Science Foundation of China (Grants No. 11634006 and No. 81127901) and by a project funded by the Priority Academic Program Development of Jiangsu Higher Education Institutions.

Y. Z. and X. F. contributed equally to this work.

- 
- [1] M. Schroeder, *Diffuse Sound Reflection by Maximum-Length Sequences*, *J. Acoust. Soc. Am.* **57**, 149 (1975).
  - [2] M. Schroeder, *Binaural Dissimilarity and Optimum Ceilings for Concert Halls: More Lateral Sound Diffusion*, *J. Acoust. Soc. Am.* **65**, 958 (1979).
  - [3] P. D’Antonio and T. Cox, *Diffusor Application in Rooms*, *Appl. Acoust.* **60**, 113 (2000).
  - [4] T. Hargreaves, T. Cox, and Y. Lam, *Surface Diffusion Coefficients for Room Acoustics: Free-Field Measures*, *J. Acoust. Soc. Am.* **108**, 1710 (2000).
  - [5] T. Cox and Y. Lam, *Prediction and Evaluation of the Scattering from Quadratic Residue Diffusers*, *J. Acoust. Soc. Am.* **95**, 297 (1994).
  - [6] X. Wang, D. Mao, W. Yu, and Z. Jiang, *Sound Barriers from Materials of Inhomogeneous Impedance*, *J. Acoust. Soc. Am.* **137**, 3190 (2015).
  - [7] F. Mahmoud, Z. Kablief, M. Mohammadreza, and N. Mahdieh, *Using the Schroeder Diffuser to Improve Parallel Noise Barriers’ Performance*, *Noise Control Engineering Journal* **62**, 210 (2014).

- [8] P. Farrehi, B. Nallamothu, and M. Navvab, *Reducing Hospital Noise with Sound Acoustic Panels and Diffusion: A Controlled Study*, *BMJ Quality Safety* **25**, 644 (2016).
- [9] J. Huang, P. Dupont, A. Undurti, J. Triedman, and R. Cleveland, *Producing Diffuse Ultrasound Reflections from Medical Instruments Using a Quadratic Residue Diffuser*, *Ultrasound Medicine Biology* **32**, 721 (2006).
- [10] J. Behrens, S. Langelier, A. Rezk, G. Lindner, L. Yeo, and J. Friend, *Microscale Anechoic Architecture: Acoustic Diffusers for Ultra Low Power Microparticle Separation via Traveling Surface Acoustic Waves*, *Lab Chip* **15**, 43 (2015).
- [11] E. Fong, N. Guilar, T. Kleeburg, H. Pham, D. Yankelevich, and R. Amirtharajah, *Integrated Energy-Harvesting Photodiodes with Diffractive Storage Capacitance*, *IEEE Trans. VLSI Syst.* **21**, 486 (2013).
- [12] P. D'Antonio and J. Konnert, *The Reflection Phase Grating Diffusor: Design Theory and Application*, *J. Audio Eng. Soc.* **32**, 228 (1984).
- [13] J. Kang, *Experimental Approach to the Effect of Diffusers on the Sound Attenuation in Long Enclosures*, *Building Acoustics* **2**, 391 (1995).
- [14] J. Kang, *Sound Propagation in Street Canyons: Comparison between Diffusely and Geometrically Reflecting Boundaries*, *J. Acoust. Soc. Am.* **107**, 1394 (2000).
- [15] L. Xiao, T. Cox, and M. Avis, *Active Diffusers: Some Prototypes and 2D Measurements*, *J. Sound Vib.* **285**, 321 (2005).
- [16] G. Ma, M. Yang, S. Xiao, Z. Yang, and P. Sheng, *Acoustic Metasurface with Hybrid Resonances*, *Nat. Mater.* **13**, 873 (2014).
- [17] Y. Li and B. M. Assouar, *Acoustic Metasurface-Based Perfect Absorber with Deep Subwavelength Thickness*, *Appl. Phys. Lett.* **108**, 063502 (2016).
- [18] J. Zhao, B. Li, Z. Chen, and C. Qiu, *Manipulating Acoustic Wavefront by Inhomogeneous Impedance and Steerable Extraordinary Reflection*, *Sci. Rep.* **3**, 2537 (2013).
- [19] Y. Li, X. Jiang, R. Li, B. Liang, X. Zou, L. Yin, and J. Cheng, *Experimental Realization of Full Control of Reflected Waves with Subwavelength Acoustic Metasurfaces*, *Phys. Rev. Applied* **2**, 064002 (2014).
- [20] Y. Xie, W. Wang, H. Chen, A. Konneker, B. I. Popa, and S. A. Cummer, *Wavefront Modulation and Subwavelength Diffractive Acoustics with an Acoustic Metasurface*, *Nat. Commun.* **5**, 5553 (2014).
- [21] K. Tang, C. Qiu, M. Ke, J. Lu, Y. Ye, and Z. Liu, *Anomalous Refraction of Airborne Sound through Ultrathin Metasurfaces*, *Sci. Rep.* **4**, 6517 (2015).
- [22] Y. Li, X. Jiang, B. Liang, J. Cheng, and L. Zhang, *Metascreen-Based Acoustic Passive Phased Array*, *Phys. Rev. Applied* **4**, 024003 (2015).
- [23] X. Zhu, K. Li, P. Zhang, J. Zhu, J. Zhang, C. Tian, and S. Liu, *Implementation of Dispersion-Free Slow Acoustic Wave Propagation and Phase Engineering with Helical-Structured Metamaterials*, *Nat. Commun.* **7**, 11731 (2016).
- [24] C. Shen, Y. Xie, J. Li, S. A. Cummer, and Y. Jing, *Asymmetric Acoustic Transmission through Near-Zero-Index and Gradient-Index Metasurfaces*, *Appl. Phys. Lett.* **108**, 223502 (2016).
- [25] Y. Zhu, X. Zou, B. Liang, and J. Cheng, *Acoustic One-Way Open Tunnel by Using Metasurface*, *Appl. Phys. Lett.* **107**, 113501 (2015).
- [26] S. A. Cummer, J. Christensen, and A. Alù, *Controlling Sound with Acoustic Metamaterials*, *Nat. Rev. Mater.* **1**, 16001 (2016).
- [27] G. Ma and P. Sheng, *Acoustic Metamaterials: From Local Resonances to Broad Horizons*, *Sci. Adv.* **2**, e1501595 (2016).
- [28] Z. Liu, X. Zhang, Y. Mao, Y. Zhu, Z. Yang, and C. T. Chan, *Locally Resonant Sonic Materials*, *Science* **289**, 1734 (2000).
- [29] L. Zigoneanu, B. I. Popa, and S. A. Cummer, *Three-Dimensional Broadband Omnidirectional Acoustic Ground Cloak*, *Nat. Mater.* **13**, 352 (2014).
- [30] B.-I. Popa and S. A. Cummer, *Non-reciprocal and Highly Nonlinear Active Acoustic Metamaterials*, *Nat. Commun.* **5**, 3398 (2014).
- [31] J. Mei, G. Ma, M. Yang, Z. Yang, W. Wen, and P. Sheng, *Dark Acoustic Metamaterials as Super Absorbers for Low-Frequency Sound*, *Nat. Commun.* **3**, 756 (2012).
- [32] N. Fang, D. Xi, J. Xu, M. Ambati, W. Srituravanich, C. Sun, and X. Zhang, *Ultrasonic Metamaterials with Negative Modulus*, *Nat. Mater.* **5**, 452 (2006).
- [33] Y. Ding, Z. Liu, C. Qiu, and J. Shi, *Metamaterial with Simultaneously Negative Bulk Modulus and Mass Density*, *Phys. Rev. Lett.* **99**, 093904 (2007).
- [34] S. Zhang, L. Yin, and N. Fang, *Focusing Ultrasound with an Acoustic Metamaterial Network*, *Phys. Rev. Lett.* **102**, 194301 (2009).
- [35] J. Li, L. Fok, X. Yin, G. Bartal, and X. Zhang, *Experimental Demonstration of an Acoustic Magnifying Hyperlens*, *Nat. Mater.* **8**, 931 (2009).
- [36] V. Garcia-Chocano, J. Christensen, and J. Sanchez-Dehesa, *Negative Refraction and Energy Funneling by Hyperbolic Materials: An Experimental Demonstration in Acoustics*, *Phys. Rev. Lett.* **112**, 144301 (2014).
- [37] C. Shen, Y. Xie, N. Sui, W. Wang, S. A. Cummer, and Y. Jing, *Broadband Acoustic Hyperbolic Metamaterial*, *Phys. Rev. Lett.* **115**, 254301 (2015).
- [38] B. Liang, S. Guo, J. Tu, D. Zhang, and J. Cheng, *An Acoustic Rectifier*, *Nat. Mater.* **9**, 989 (2010).
- [39] X. Jiang, Y. Li, B. Liang, J. Cheng, and L. Zhang, *Convert Acoustic Resonances to Orbital Angular Momentum*, *Phys. Rev. Lett.* **117**, 034301 (2016).
- [40] Y. Zhu, X. Zou, R. Li, X. Jiang, J. Tu, B. Liang, and J. Cheng, *Dispersionless Manipulation of Reflected Acoustic Wavefront by Subwavelength Corrugated Surface*, *Sci. Rep.* **5**, 10966 (2015).
- [41] G. Ward, R. Lovelock, A. Murray, A. Hibbins, J. Sambles, and J. Smith, *Boundary-Layer Effects on Acoustic Transmission through Narrow Slit Cavities*, *Phys. Rev. Lett.* **115**, 044302 (2015).
- [42] M. Serra-Garcia and C. Daraio, *Visco-Thermal Effects in Acoustic Metamaterials: From Total Transmission to Total Reflection and High Absorption*, *New J. Phys.* **18**, 033003 (2016).

- [43] T. Cox and P. D'Antonio, *Acoustic Absorbers and Diffusers: Theory, Design and Application*, 3rd ed. (CRC Press, Boca Raton, FL, 2016).
- [44] A. Jrvinen, L. Savioja, and K. Melkas, *Numerical Simulations of the Modified Schroeder Diffuser Structure*, *J. Acoust. Soc. Am.* **103**, 3065 (1998).
- [45] F.P. Mechel, *The Wide-Angle Diffuser—A Wide-Angle Absorber?*, *Acta Acustica* **81**, 379 (1995).
- [46] J.A. Hargreaves and T.J. Cox, *Improving the Bass Response of Schroeder Diffuser*, *Proc. Inst. Acoust.* **25**, 199 (2003).
- [47] P. D'Antonio and T.J. Cox, *Extended Bandwidth Folded Well Diffusor*, US Patent No. 7322441 (29 January 2008).
- [48] K. Fujiwara, K. Nakai, and H. Torihara, *Visualisation of the Sound Field around a Schroeder Diffuse*, *Appl. Acoust.* **60**, 225 (2000).
- [49] T. Wu, T.J. Cox, and Y.W. Lam, *A Profiled Structure with Improved Low Frequency Absorption*, *J. Acoust. Soc. Am.* **110**, 3064 (2001).
- [50] See Supplemental Material at <http://link.aps.org/supplemental/10.1103/PhysRevX.7.021034> for [brief description].
- [51] T. Cox, B. Dalenback, P. D'Antonio, J. Embrechts, J. Jeon, E. Mommertz, and M. Vorländer, *A Tutorial on Scattering and Diffusion Coefficients for Room Acoustic Surfaces*, *Acta Acustica* **92**, 1 (2006).